Supplementary Materials for

Hyperbolic graphene framework with optimum efficiency for conductive composites

Xiaoting Liu[†], Kai Pang[†], Yingjun Liu, Chao Gao, Zhen Xu[*]

MOE Key Laboratory of Macromolecular Synthesis and Functionalization, Department of Polymer Science and Engineering, Key Laboratory of Adsorption and Separation Materials & Technologies of Zhejiang Province, Zhejiang University, 38 Zheda Road, Hangzhou 310027, China.

*Corresponding author. Email: zhenxu@zju.edu.cn.

Supporting figures

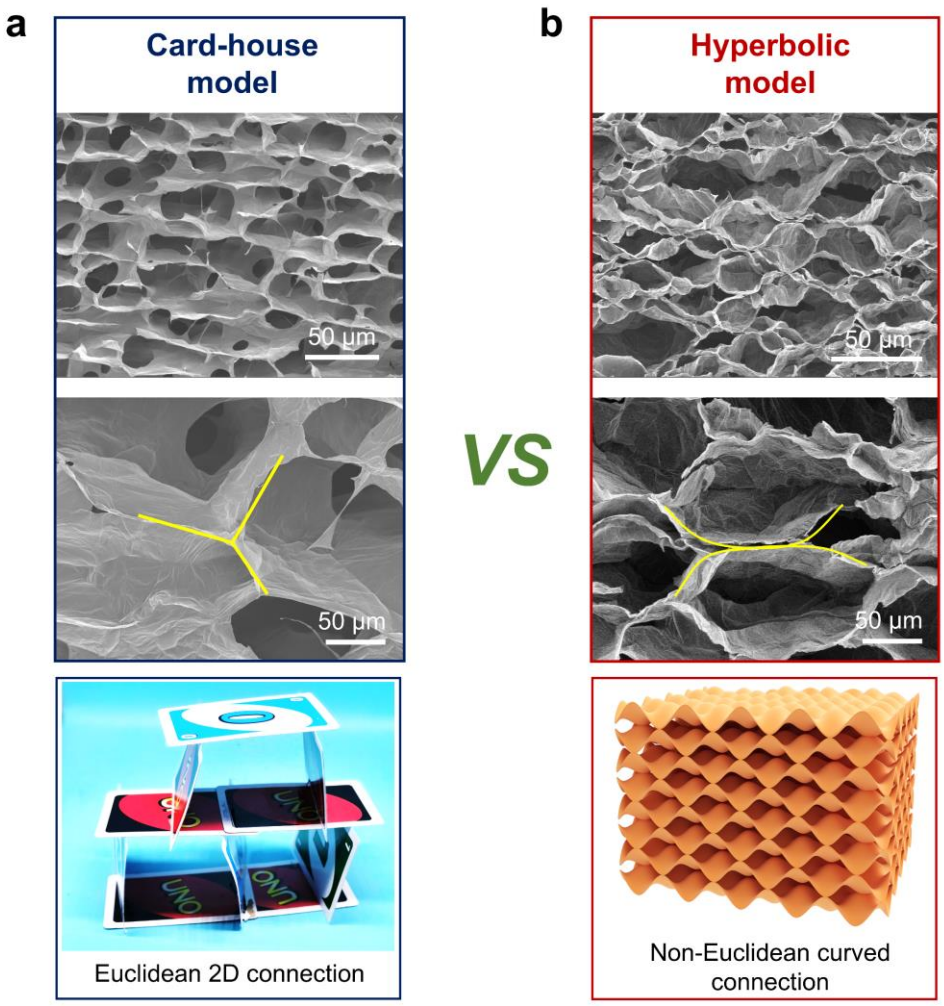

Figure S1. Polyhedral "card-house" model (by conventional methods) and hyperbolic model (by hydroplastic foaming) of 3D graphene framework. Photo Credit: Kai Pang, Zhejiang University.

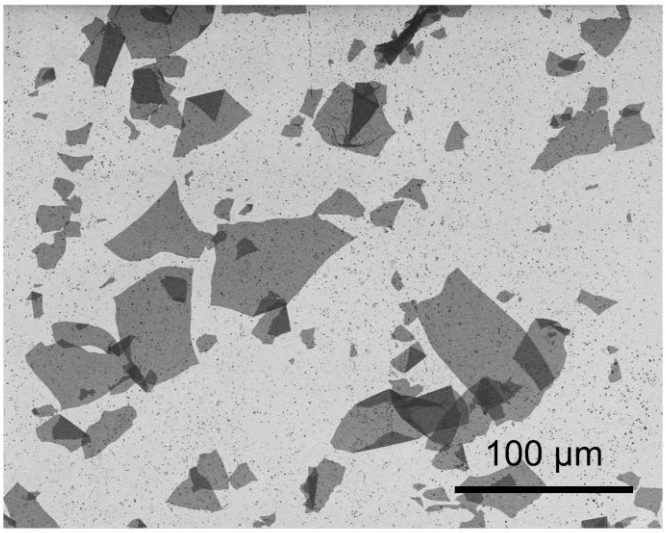

Figure S2. SEM image of GO sheets.

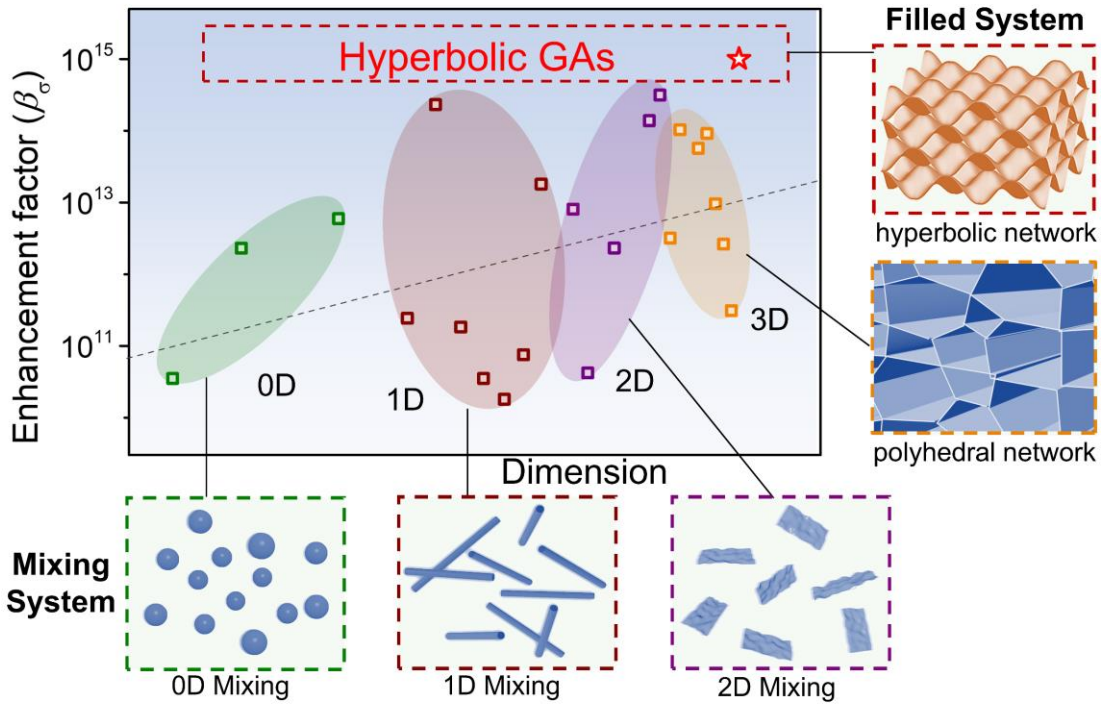

Figure S3. Electrical enhancement factor of composites with different nanofillers[1-21].

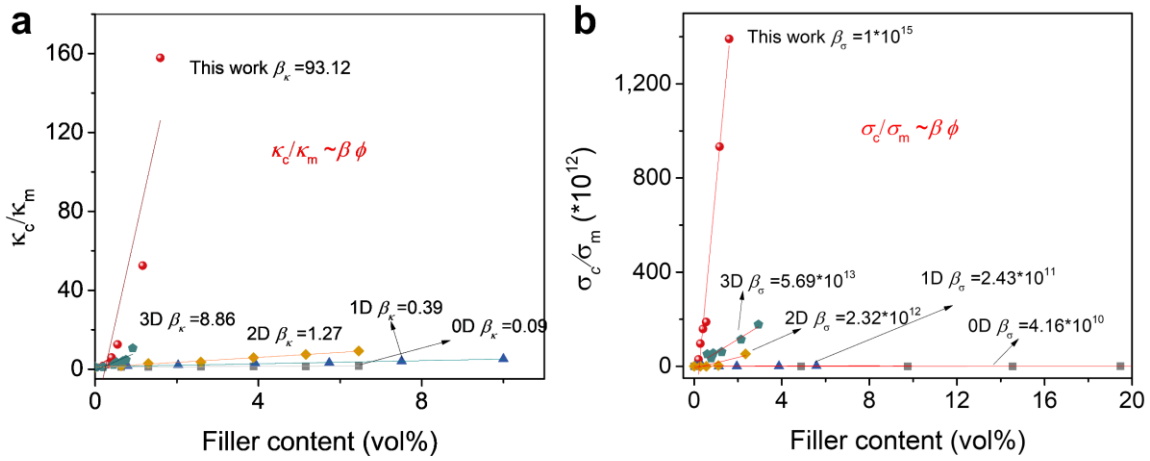

Figure S4. Comparison of typical enhancement factors of 0D, 1D, 2D and 3D nanofillers[1-3,16,22,23].

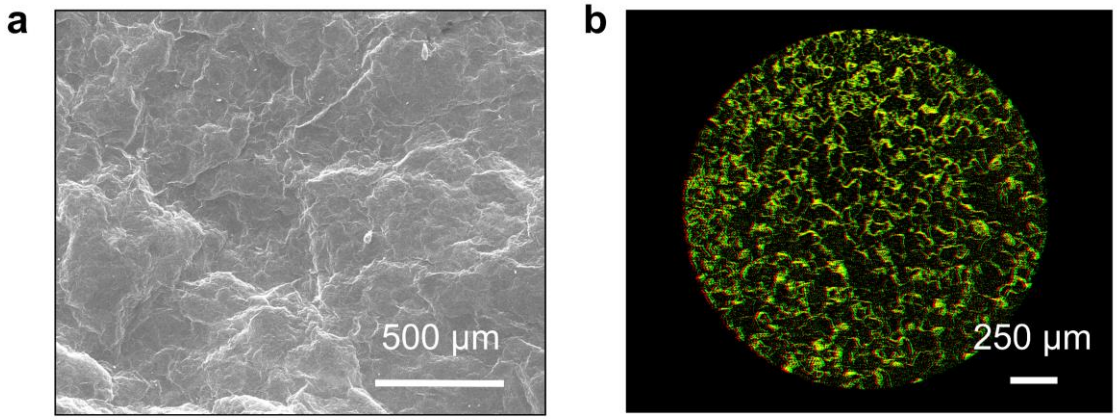

Figure S5. (a) SEM and **(b)** CT images of the surface of HGA.

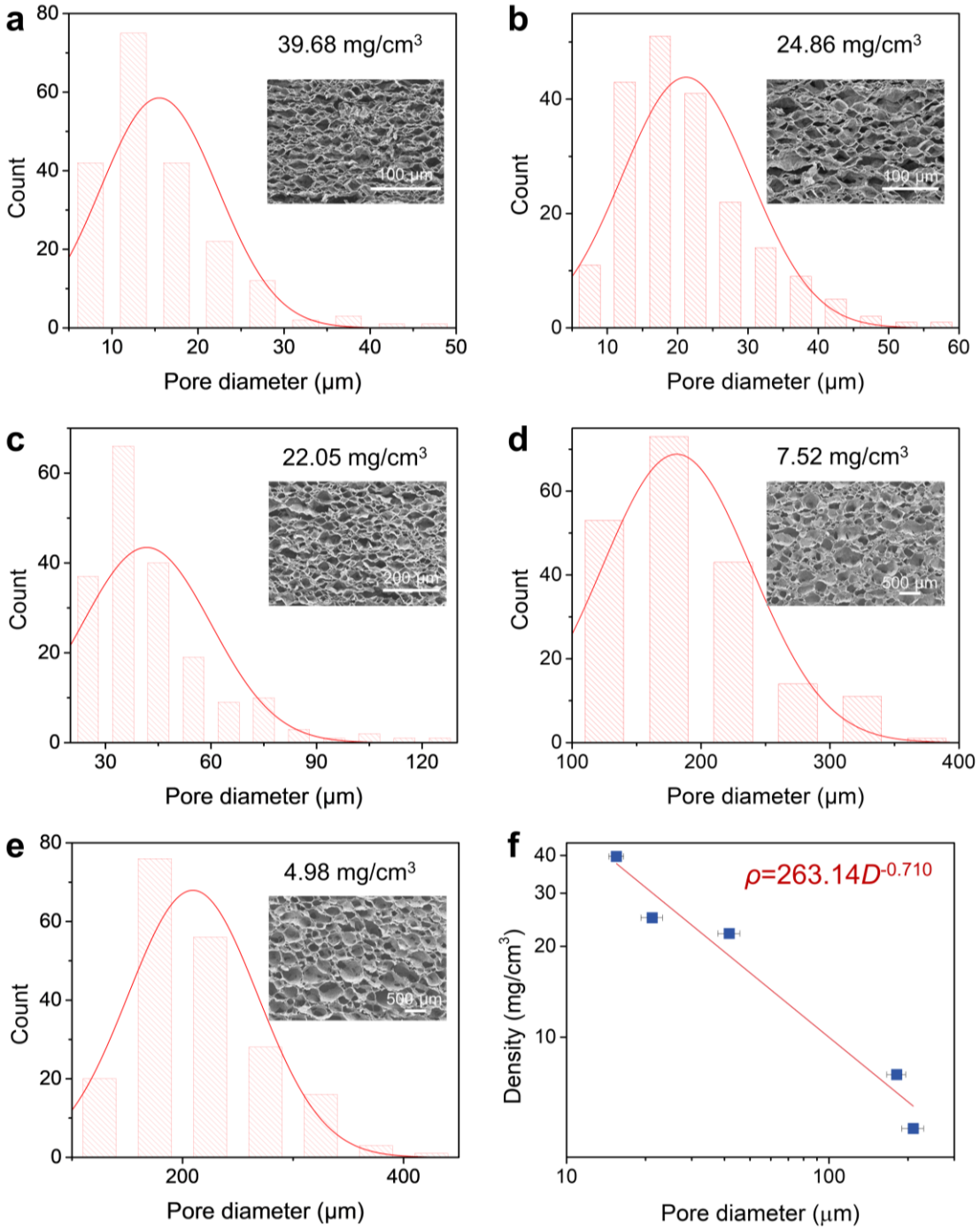

Figure S6. (a-e) Pore size distributions of HGAs with different densities. (f) Densities of HGAs as a function of pore sizes.

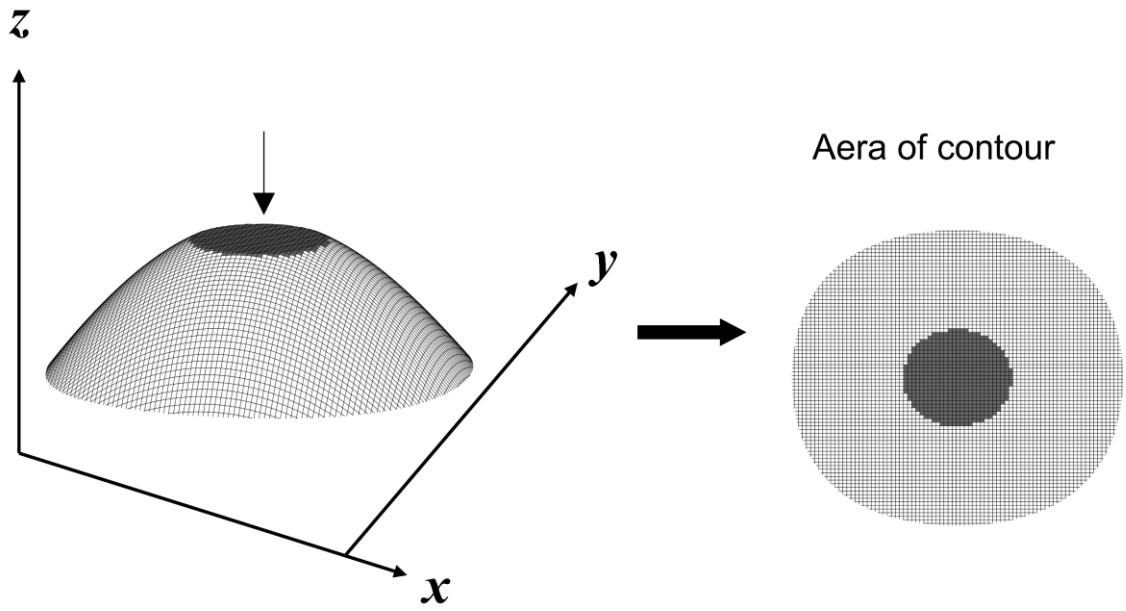

Figure S7. Side and top view of the contact area between curved graphene sheets.

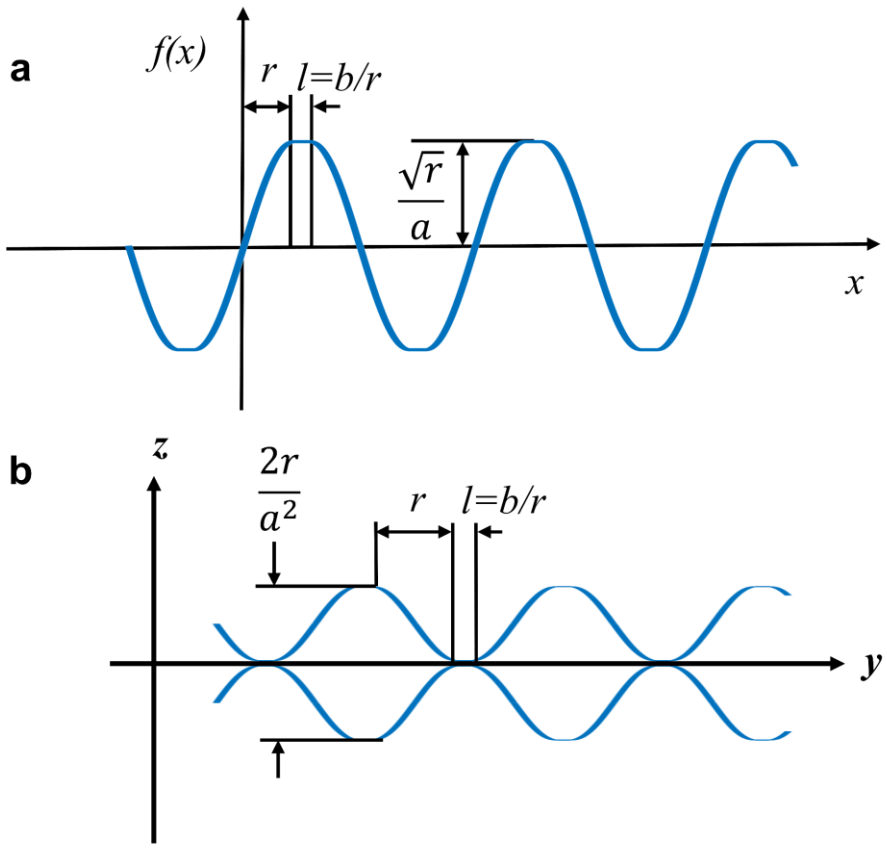

Figure S8. Model calculation of contact area of hyperbolic graphene networks.

Based on previous report, the modified model is proposed as followed in Figure S8A:

$$f(x) = \begin{cases} -\frac{\sqrt{r}}{a},\ x \in [-\frac{k}{2}(r+l),\ -\frac{kr}{2}) \\ \frac{\sqrt{r}}{a}\sin\left(\frac{\pi x}{r}\right),\ x \in [-\frac{kr}{2}, \frac{kr}{2}) \\ \frac{\sqrt{r}}{a},\ x \in [\frac{kr}{2}, \frac{k}{2}(r+2l)) \\ \frac{\sqrt{r}}{a}\sin[\frac{\pi(x-l)}{r}],\ x \in [\frac{k}{2}(r+2l),\ \frac{k}{2}(3r+2l)) \\ -\frac{\sqrt{r}}{a},\ x \in [\frac{k}{2}(3r+2l), \frac{3k}{2}(r+l)) \end{cases}$$

$$f(y) = \begin{cases} -\frac{\sqrt{r}}{a},\ y \in [-\frac{k}{2}(r+l),\ -\frac{kr}{2}) \\ \frac{\sqrt{r}}{a}\sin\left(\frac{\pi y}{r}\right),\ y \in [-\frac{kr}{2}, \frac{kr}{2}) \\ \frac{\sqrt{r}}{a},\ y \in [\frac{kr}{2}, \frac{k}{2}(r+2l)) \\ \frac{\sqrt{r}}{a}\sin[\frac{\pi(y-l)}{r}],\ y \in [\frac{k}{2}(r+2l),\ \frac{k}{2}(3r+2l)) \\ -\frac{\sqrt{r}}{a},\ y \in [\frac{k}{2}(3r+2l), \frac{3k}{2}(r+l)) \end{cases}$$

where a and b are the coefficients related to the HGA geometry, k $\propto$ Z (arbitrary integer).
As shown in Figure S8B, because hyperbolic curvature follows Gaussian curvature characteristics, so
$z\,(x,y)\ = f(x) * f(y)$
The contact area of a cell in parallel direction: $S_c = l^2$, $(l = b/r)$
The surface area of a cell: S= $\iint \sqrt{1 + \left(\frac{dz}{dx}\right)^2 + \left(\frac{dz}{dy}\right)^2}\, dxdy$
The volume of a cell: $V = \left(\frac{2\sqrt{r}}{a}\right)^2 * (2r\ + 2l) * (2r + 2l)$
The density of HGA: $\rho = S{*}t{*}2.26/V$, t is the thickness of the pore wall.

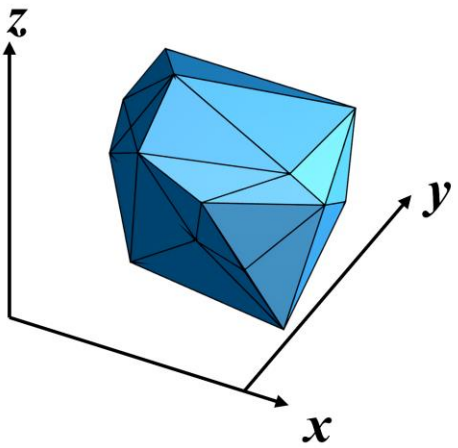

Figure S9. Theoretical calculation of contact area of polyhedral graphene networks.

In order to describe the random structure of GAs, taking randomly distributed points in the unit space as the body center, we learn from the generation principle of Tyson polyhedrons to generate a convex polyhedron with random structures as shown in Figure S9.
The length of the three sides of each plane：

$$a_i = B_iC_i = \sqrt{(x_{2i} - x_{3i})^2 + (y_{2i} - y_{3i})^2 + (z_{2i} - z_{3i})^2}$$
$$b_i = A_iC_i = \sqrt{(x_{1i} - x_{3i})^2 + (y_{1i} - y_{3i})^2 + (z_{1i} - z_{3i})^2}$$
$$c_i = A_iB_i = \sqrt{(x_{1i} - x_{2i})^2 + (y_{1i} - y_{2i})^2 + (z_{1i} - z_{2i})^2}$$
$$Sc = t * \Sigma p_i,\ \ p_i = a_i + b_i + c_i$$
$$S = \Sigma S_i,\ S_i = \frac{\sqrt{p_i * (p_i - a_i) * (p_i - b_i) * (p_i - c_i)}}{4}$$
$$\rho = S * t * 2.26/V$$

The volume V of the resulting polyhedron is dependent on the randomly distributed points in the unit space.

According to the above formula, the contact area between graphene sheets is obtained as shown in Fig. 2H.

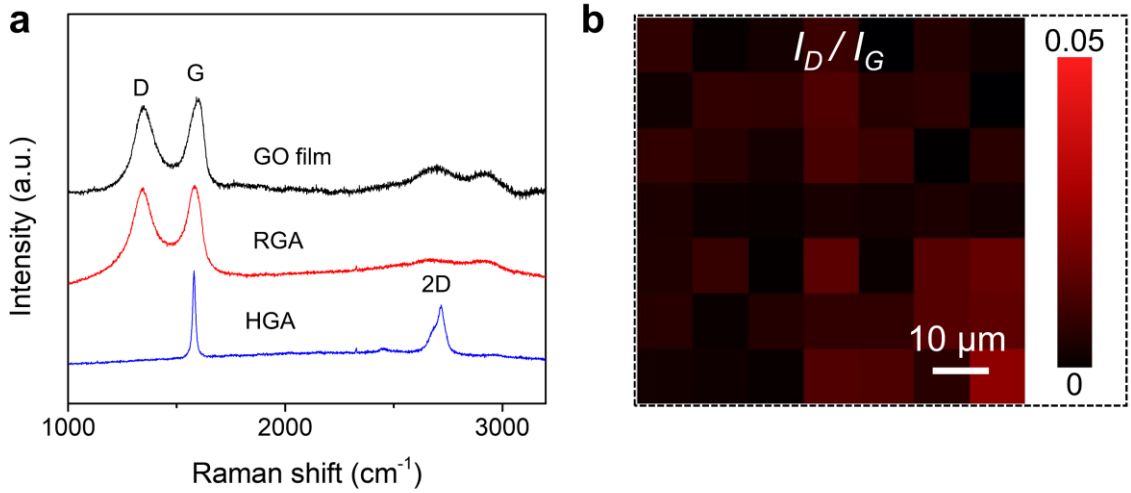

Figure S10. Raman characterization. (a) Raman spectra of GO film, RGA and HGA. (b) Raman mapping of HGA.

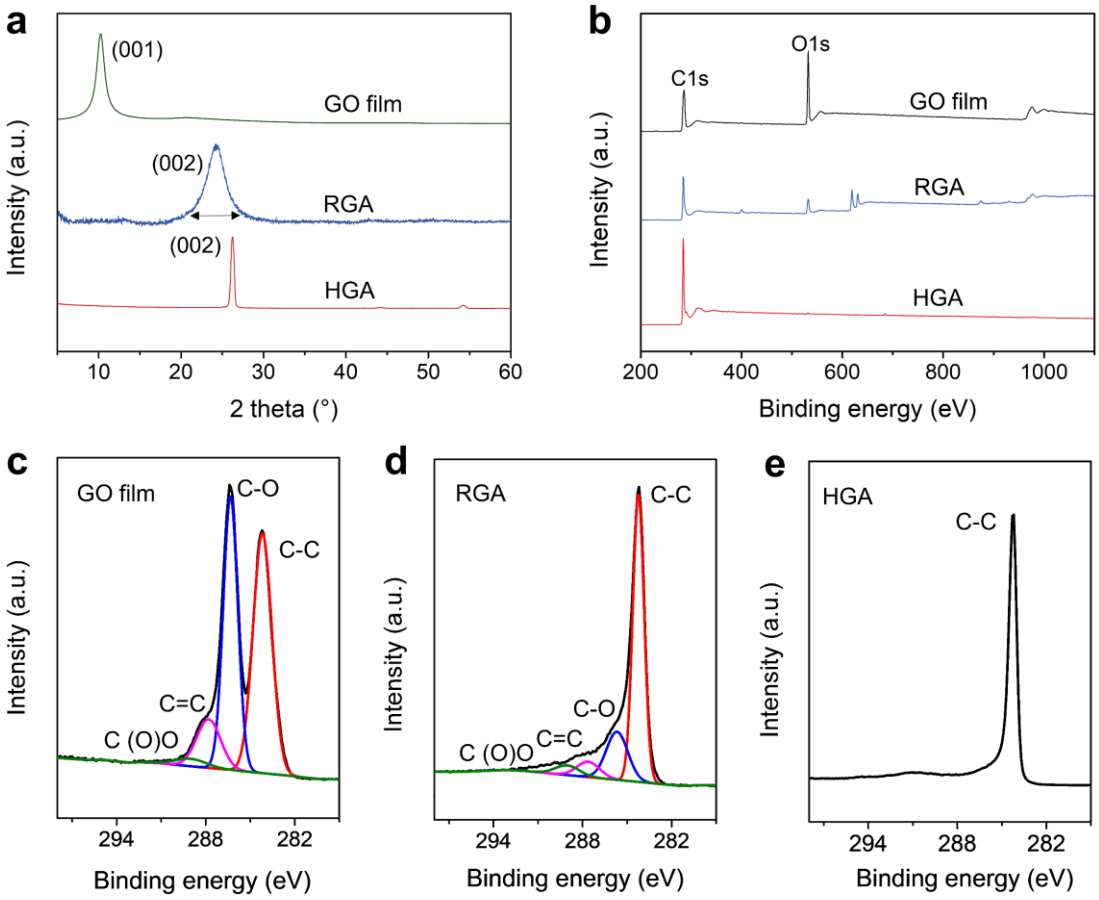

Figure S11. (a) XRD patterns and (b-e) XPS spectrum of GO film, RGA and HGA.

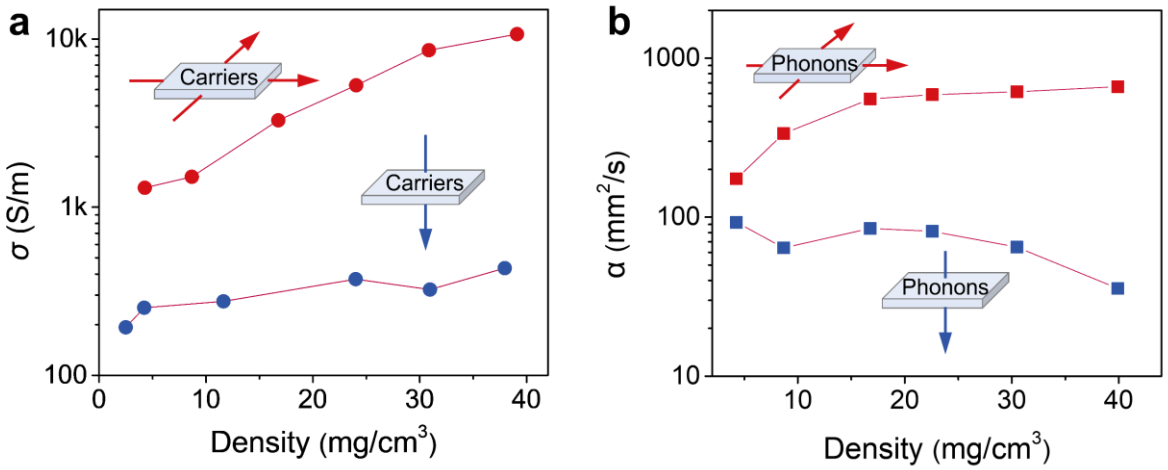

Figure S12. (a) The in-plane and through-plane electrical conductivity and (b) thermal diffusion coefficient of HGAs.

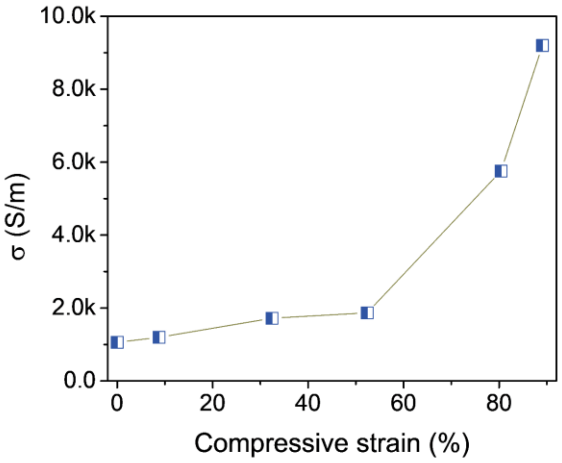

Figure S13. Electrical conductivity of HGA with different compressive strains.

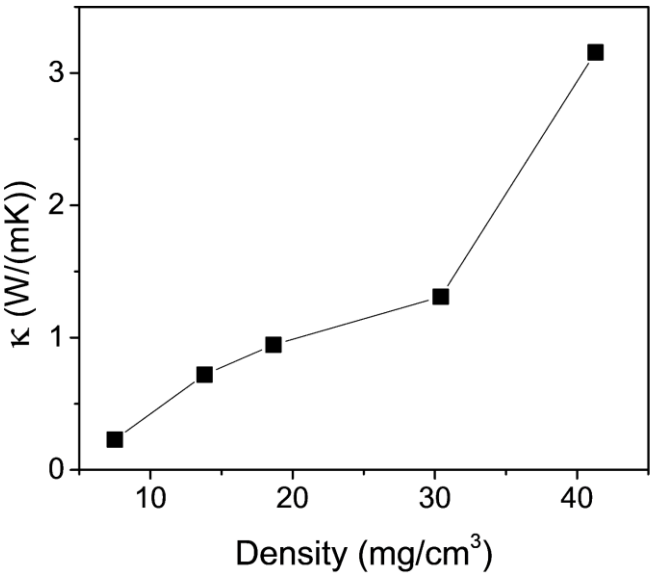

Figure S14. Thermal conductivity of freeze-dried GAs with different densities.

Figure S15. The digital photo of PGC after vacuum infusion. Photo Credit: Kai Pang, Zhejiang University.

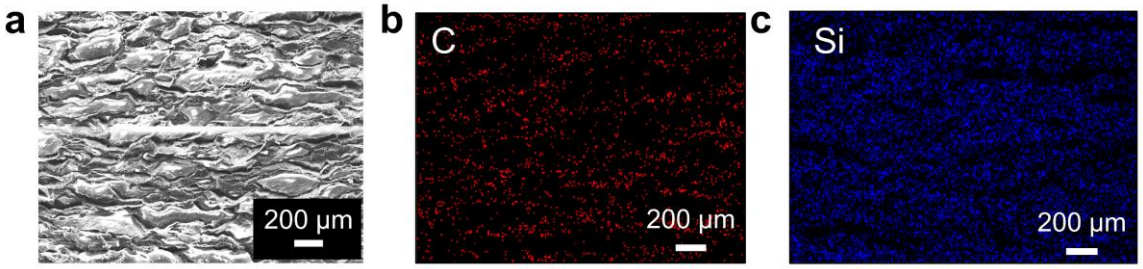

Figure S16. Elemental mappings of PGC. (a) SEM mapping image. Elemental (b) C and (c) Si mapping images.

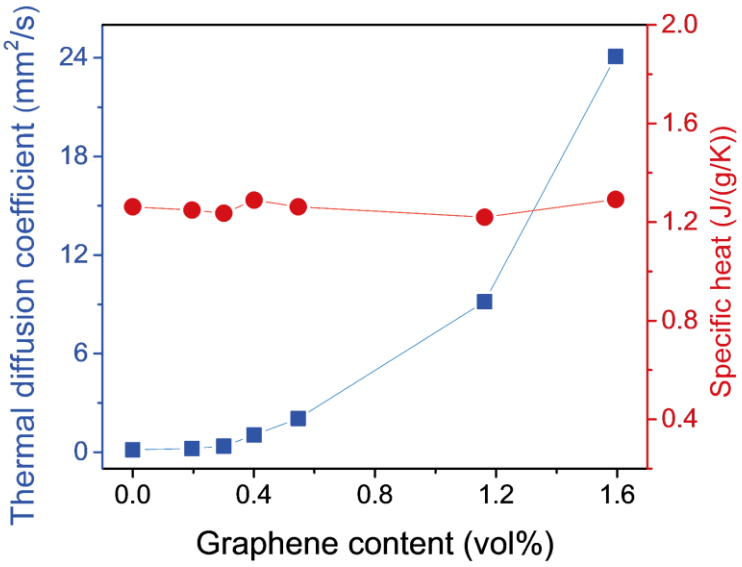

Figure S17. Thermal diffusion coefficient and specific heat of PGCs with different graphene loadings.

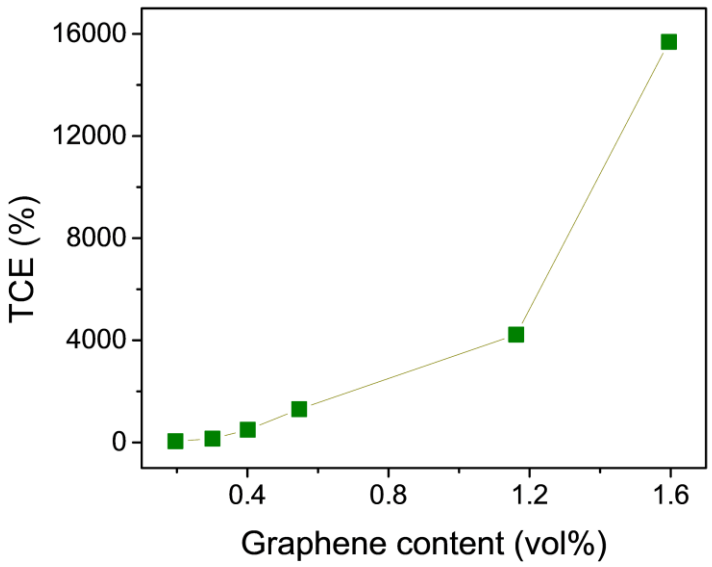

Figure S18. TCE of PGCs with different graphene loadings.

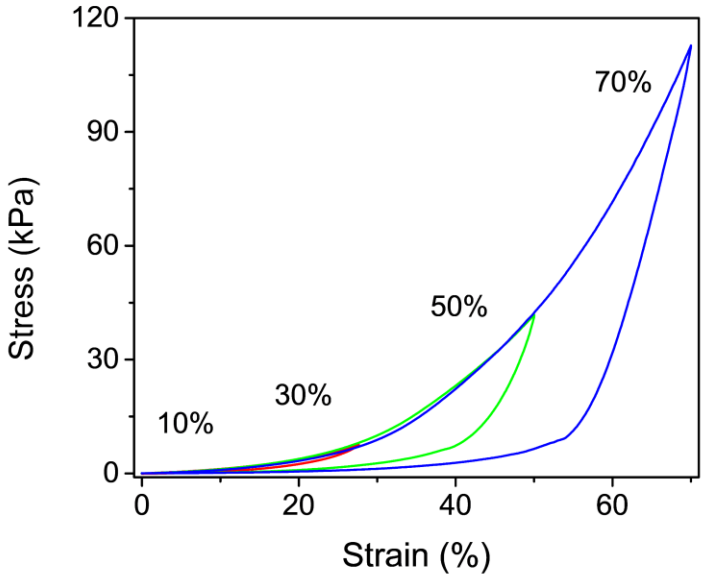

Figure S19. The compressive curves of PGC at various strains.

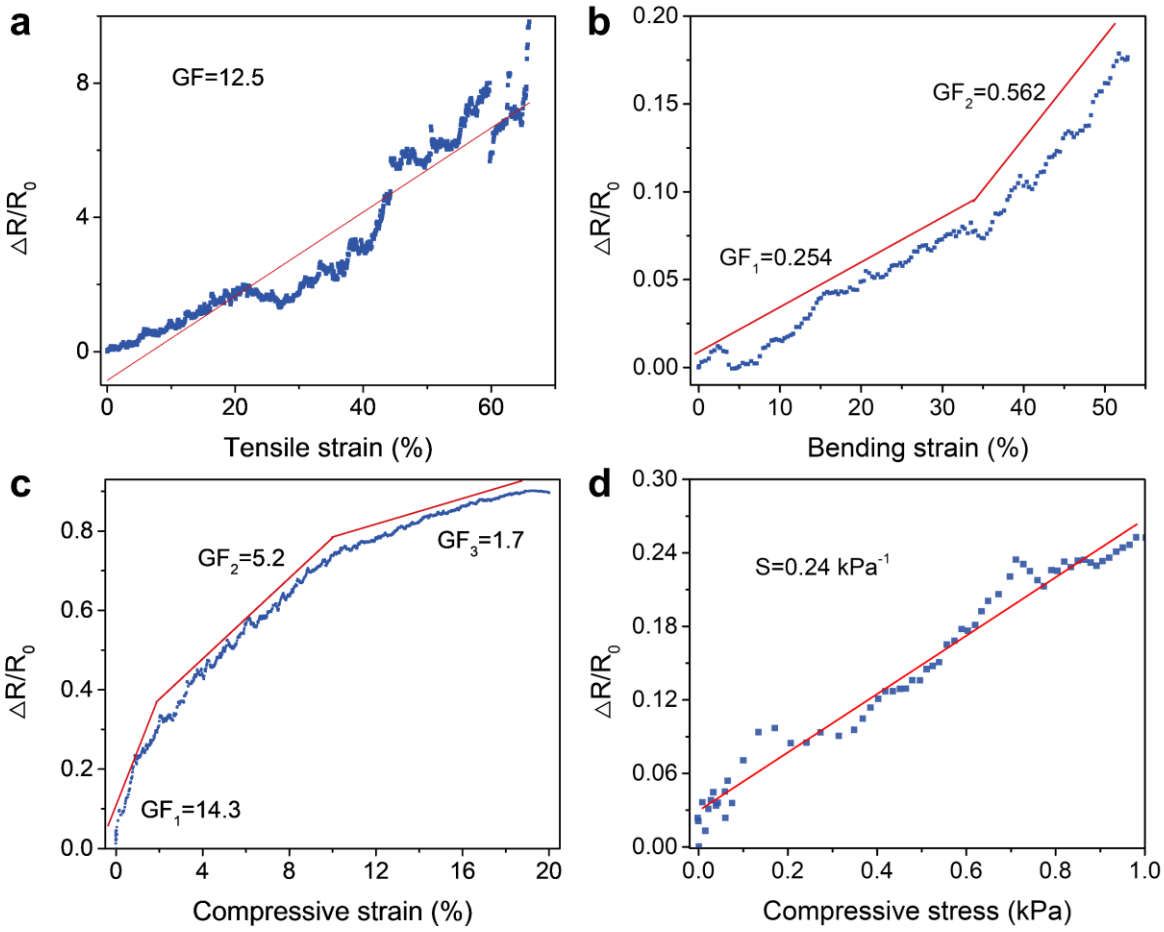

Figure S20. The $\Delta R/R_0$ changes of PGC with (a) tensile strain, (b) bending strain, (c) compressive strain and (d) compressive stress.

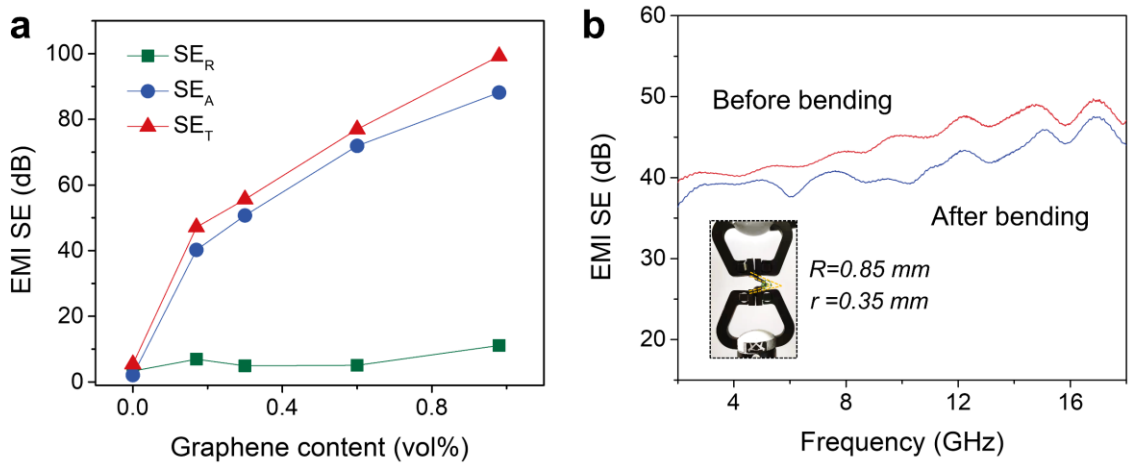

Figure S21. EMI SE and mechanical stability of PGC. (a) Average SE_T, SE_R, and SE_A of the PGCs with various graphene loadings. (b) EMI SE values of PGC before and after bending 1000 cycles. Photo Credit: Kai Pang, Zhejiang University.

Supporting movies

Movie S1.

Heat diffusion of PDMS and PGC for a high-power LED lamp. Play speed is 10x of the actual speed.

Movie S2.

Heat transfer of PDMS and PGC for a high-power LED lamp. Play speed is 10x of the actual speed.

Supporting references

1. Ram, R., Soni, V. & Khastgir, D. Electrical and thermal conductivity of polyvinylidene fluoride (PVDF)–conducting carbon black (CCB) composites: Validation of various theoretical models. *Composites Part B.* **185,** 107748 (2020).

2. Shen, X. et al. Three-dimensional multilayer graphene web for polymer nanocomposites with exceptional transport properties and fracture resistance. Mater. Horiz. 5, 275-284 (2018).

3 Huang, Y. et al. The influence of single-walled carbon nanotube structure on the electromagnetic interference shielding efficiency of its epoxy composites. *Carbon* **45,** 1614–1621 (2007).

4. Regev, O., ElKati, P. N. B., Loos, J. & Koning, C. E. Preparation of conductive nanotube-polymer composites using latex technology. *Adv. Mater.* **16,** 248-251 (2004).

5. Li, J. et al. Correlations between percolation threshold, dispersion state, and aspect ratio of carbon nanotubes. *Adv. Funct. Mater.* **17,** 3207–3215 (2007).

6. Ram, R., Rahaman, M. & Khastgir, D. Electrical properties of polyvinylidene fluoride (PVDF)/multi-walled carbon nanotube (MWCNT) semi-transparent composites: Modelling of DC conductivity. *Composites Part A* **69,** 30–39 (2015).

7. Yousefi, N. et al. Highly aligned graphene/polymer nanocomposites with excellent dielectric properties for high-performance electromagnetic interference shielding. *Adv. Mater.* **26,** 5480–5487 (2014).

8. Chen, M. T. et al. Highly stretchable conductors integrated with a conductive carbon nanotube/graphene network and 3D porous poly(dimethylsiloxane). *Adv. Funct. Mater.* **24,** 7548–7556 (2014).

9. Chen, Z. P., Xu, C., Ma, C. Q., Ren, W. C. & Cheng, H. M. Lightweight and flexible graphene foam composites for high-performance electromagnetic interference shielding. *Adv. Mater.* **25,** 1296–1300 (2013).

10. Pelíˇsková, M., Piyamanocha, P., Prokeˇs, J., Varga, M. & Sáha, P. The electrical conductivity of ethylene butyl-acrylate/carbon black composites: The effect of foaming on the percolation threshold. *Synth. Met.* **188,** 140–145 (2014).

11. Krückel, J., Starý, Z., Triebel, C., Schubert, D. W. & Münstedt, H. Conductivity of polymethylmethacrylate filled with carbon black or carbon fibres under oscillatory shear. *Polymer* **53,** 395-402 (2012).

12. Ma, P. C. et al. Enhanced electrical conductivity of nanocomposites containing hybrid fillers of carbon nanotubes and carbon black. *ACS Appl. Mater. Interfaces* **1,** 1090-1096 (2009).

13. Kim, Y. J. et al. Electrical conductivity of chemically modified multiwalled carbon nanotube/epoxy composites. *Carbon* **43,** 23–30 (2005).

14. Aguilar, J. O., Bautista-Quijano, J. R. & Avilés, F. Influence of carbon nanotube clustering on the electrical conductivity of polymer composite films. *eXPRESS Polym. Lett.* **4,** 292–299 (2010).

15. Zhang, H. B., Zheng, W. G., Yan, Q., Jiang, Z. G. & Yu, Z. Z. The effect of surface chemistry of graphene on rheological and electrical properties of polymethylmethacrylate composites. *Carbon* **50,** 5117–5125 (2012).

16. Yoonessi, M. & Gaier, J. R. Highly conductive multifunctional graphene polycarbonate nanocomposites. *ACS Nano* **4,** 7211-7220 (2010).

17. Zhang, H. B. et al. Electrically conductive polyethylene terephthalate/graphene nanocomposites prepared by melt compounding. *Polymer* **51,** 1191–1196 (2010).

18. Qi, X. Y. et al. Enhanced electrical conductivity in polystyrene nanocomposites at ultra-low graphene content. *ACS Appl. Mater. Interfaces* **3,** 3130–3133 (2011).

19. Chen, G. Q., Liu, Y. X., Liu, F. & Zhang, X. Fabrication of three-dimensional graphene foam with high electricalconductivity and large adsorption capability. *Appl. Surf. Sci.* **311,** 808-815 (2014).

20. Wang, Z. Y. et al. Graphene aerogel/epoxy composites with exceptional anisotropic structure and properties. *ACS Appl. Mater. Interfaces* **7,** 5538-5549 (2015).

21. Fan, Z., Gong, F., Nguyen, S. T. & Duong, H. M. Advanced multifunctional graphene aerogel – Poly (methyl methacrylate) composites: Experiments and modeling. *Carbon* **81,** 396–404 (2015).

22. Bonnet, P., Sireude, D., Garnier, B. & Chauvet, O. Thermal properties and percolation in carbon nanotube-polymer composites. *Appl. Phys. Lett.* **91,** 201910 (2007).

23. Song, S. H. et al. Enhanced thermal conductivity of epoxy–graphene composites by using non-oxidized graphene flakes with non-covalent functionalization. *Adv. Mater.* **25,** 732–737 (2013).